Generic Air-gen Effect in Nanoporous Materials for Sustainable Energy Harvesting from Air Humidity

Xiaomeng Liu[1], Hongyan Gao[1], Lu Sun,[1] Jun Yao[1,2,3]*

1. Department of Electrical Computer and Engineering, University of Massachusetts, Amherst, MA 01003, USA.
2. Institute for Applied Life Sciences (IALS), University of Massachusetts, Amherst, MA 01003, USA.
3. Department of Biomedical Engineering, University of Massachusetts, Amherst, MA 01003, USA.

* Corresponding author. Email: juny@umass.edu (J.Y.)

ABSTRACT

Air humidity is a vast, sustainable reservoir of energy that, unlike solar and wind, is continuously available. However, previously described technologies for harvesting energy from air humidity are either not continuous or require unique material synthesis or processing, which has stymied scalability and broad deployment. Here, we report a generic effect for continuous energy harvesting from air humidity, which can be applied to a broad range of inorganic, organic, and biological materials. The common feature of these materials is that they are engineered with appropriate nanopores to allow air water to pass through and undergo dynamic adsorption-desorption exchange at the porous interface, resulting in surface charging. The top exposed interface experiences such dynamic interaction more than the bottom sealed interface in a thin-film device structure, yielding a spontaneous and sustained charging gradient for continuous electric output. Analyses of material properties and electric outputs lead to a 'leaky capacitor' model that can describe how electricity is harvested and predict current behaviors consistent with experiments. Predictions from the model guide the fabrication of devices made from heterogeneous junctions of different material combinations to further expand the device category. The work opens a wide door for the broad exploration of sustainable electricity from ambient air.

1. Introduction

Energy harvesting from environmental sources can mitigate threats associated with fossil fuels and provide flexible powering solutions for the broad deployment of the Internet of Things.[1-2] While hydroelectricity has been an important part of clean energy, its requirement for a large body of water and specific geographical condition limits its broad applicability.[3] On the other hand, air water or humidity is much more accessible and forms a large, ubiquitous, sustainable energy source.[4-5] As a result, several emerging technologies have been designed for harvesting energy from air humidity.[4-7]

The general strategy is to induce an imbalance in charge distribution at the water-solid interface of materials to drive charge flow for electricity.[4] Previous approaches mainly fall into three categories. The first involves creating directional water flow that carries along interfacial charge flow for current. An external humidity gradient is applied to drive the water flow, but this requires specific location (*e.g.*, water surface) or only yields a short burst of current if the applied humidity gradient is not sustained (*e.g.*, breathing).[8-10] In either case, it falls short of scalable deployment in the ambient environment. The second involves introducing heterogenous surfaces in material by functionalization[11-12] or coating,[13-14] which can yield differentiated interfacial charge distribution at the same humidity level. This approach can generate current in the ambient environment, although the heterogenous surface engineering can increase processing costs and limit long-term stability.[15-16] The third approach uses initially dehydrated materials to adsorb air water, during which the temporarily induced adsorption gradient can drive electric output.[17-18] However, once adsorption saturation is reached, the gradient disappears and the electric output ceases. These devices offered a one-time current output no longer than 48 h.[17-18]

Recently, it was discovered that a homogenous thin film made from (non-dehydrated) protein nanowires harvested from microbe *Geobacter sulfurreducens* can generate electricity from ambient air humidity with improved energy density and long-term stability.[19] The sustainability was further demonstrated by integrating the devices into neuromorphic interfaces for self-sustainability in the ambient environment.[20] A distinct mechanism was revealed, in which a spontaneous water adsorption gradient was found to build up across the film thickness (Figure 1a) and induce differentiated charge interaction for current.[19] Importantly, the adsorption gradient maintained over time (*e.g.*, beyond a 10-month test window), showing a sustainable mechanism. This is inherently different from energy releasing in other devices, in which the temporary adsorption gradient disappeared when the initially dehydrated materials reached full adsorption and the energy output ceased.[17-18, 21] To differentiate the protein nanowire device from other devices in the broad category of humidity generators, we term the device an 'air generator' (or 'Air-gen') to highlight its sustainable feature in the ambient air environment.

A potential limitation of scaling up the Air-gen is the cost associated with the biological production of the protein nanowires. Although strategy for improved production of the protein nanowires with *Escherichia coli* has been described,[22-23] the required mass cultivation of the microbe and harvesting of the nanowires is likely to be still limited. Therefore, we intend to investigate whether the Air-gen can function with various substitutes for the protein nanowires.

2. Result and Discussion

2.1. Characteristics of an Air-gen functional material

It was analyzed that high-density nanopores, coupled by a hydrophilic interaction, induced vapor pressure lowering in the inner layers of assembled nanowire film.[19],[24] The resultant vapor-pressure gradient led to a water-adsorption gradient across the thin film thickness. The reason is that water adsorption at a solid surface is a dynamic equilibrium between adsorption and desorption, and the adsorption decreases with the decrease in the molecular concentration of air water or the vapor pressure.[25]

We will now turn to a confinement effect in gas for further understanding of the process. When the nanopore size is less than the mean free path of air-water molecule (~100 nm in the ambient environment[26]), gas-solid interaction will dominate over gas-gas interaction, leading to a thermodynamic equilibrium that deviates from free gas.[27] Previous studies have shown that gas confined in a nanoscale space has higher pressure than that in free space at the same density and temperature.[26-29] Therefore, the gas density in a confined nanospace tends to be lower than that in the open environment under equilibrium (*e.g.*, same pressure and temperature). In an alternative view, the increased chemical potential in gas (*e.g.*, from surface interaction) is balanced by its density reduction under equilibrium. Consequently, the increasing confinement deeper into the film thickness is expected to yield a reverse gradient in air-water density (Figure 1b). In other words, nanowires near the top/outer surface will come into contact with air-water molecules more often than inner/bottom nanowires. As adsorption increases with the increase in contact rate,[25] the outer nanowires will adsorb more water than inner ones to generate an adsorption gradient. Importantly, this adsorption gradient is sustained over time because it results from a dynamic equilibrium.

These mechanistic considerations suggest that other porous materials could substitute for protein nanowires as the functional material in the Air-gen device if they have: 1) a pore size comparable to or less than the mean free path of an air-water molecule, and 2) a surface that interacts with water molecules. Previous devices have always involved the use of protein nanowires.[19-20, 30] Here, we reveal a generic Air-gen effect across a broad range of organic, inorganic, and biological materials.

2.2. Observation of Air-gen effect with different materials

We began our exploration by investigating cellulose nanofibers (CNF), which have a distinct composition from protein nanowires but share some similar structural properties, such as a nanometer-scale diameter and a hygroscopic surface.[31] The assembled thin films had nanopores consistent with a previous report,[31] as shown in Figure 2a-i. Electrical measurements confirmed a spontaneous voltage output (V_o) ~260 mV (Figure 2a-ii) from the fabricated thin film device (inset; Figure S1, Supporting Information) in the ambient environment, providing initial evidence for the generic mechanistic picture shown in Figure 1.

We analyzed the water adsorption in CNF films of varying thicknesses (Figure S2, Supporting Information) and found a consistent trend of decreasing weight-percent water adsorption (W_{H2O}%) with increasing film thickness (Figure 2a-iii, blue curve). Specifically, W_{H2O}% reduced from ~24% for thin films (~5 μm thick) to ~10% for thicker ones (≥ 20 μm thick). This trend is consistent with the expected adsorption gradient,[19] with local adsorption decreasing from the outer to inner interface and resulting in different average adsorptions (W_{H2O}%) for different film thicknesses. As the film thickness increased from 5 to 25 μm, V_o also increased from ~40 to ~340 mV (Figure 2a-iii, black curve). For better comparison, we extracted the adsorption difference (ΔW_{H2O}%) between the top and bottom interfaces in CNF films and compared with V_o (Figure 2a-iv), revealing a close correlation between them. This correlation is consistent with the prediction based on a diffusion model,[19] suggesting that the output voltage is proportional to the ionization difference that correlates with adsorption difference.

A device made with nanoporous silk fibroin (SF) film[32] (Figure 2b-i; Figure S1, Supporting Information) also produced a stable V_o (~150 mV) in the ambient environment (Figure 2b-ii). The trend of decreasing W_{H2O}% with increasing film thickness was also observed, with W_{H2O}% decreasing from ~24% in thin (~5 μm) films to ~12% in thicker (> 20 μm) ones (Figure 2b-iii, blue curve). V_o increased from ~100 to 260 mV (Figure 2b-iii, black curve). The extracted ΔW_{H2O}% showed a close correlation with V_o (Figure 2b-iv). Similarly, a device made from a biofilm assembled from microorganism *G. suffurendences*[30] (Figure 2c-i; Figure S1, Supporting Information) generated a spontaneous V_o ~550 mV

(Figure 2c-ii). Similar trends of thickness-dependent W_{H2O}% (Figure 2c-iii, blue curve), V_o (black curve), and V_o-ΔW_{H2O}% correlation (Figure 2c-iv) were observed.

We then extended our study to nonbiological materials and began with thin films made from graphene oxides (GOx) flakes[33] (Figure 2d-i). Previous devices that utilized GOx layers required an applied humidity gradient or an engineering surface gradient to generate electric output.[11-12] However, we found that a homogenous GOx film can spontaneously generate a V_o ~100 mV in the ambient environment (Figure 2d-ii; Figure S1, Supporting Information). Thickness-dependent water adsorption trend was consistently observed in GOx films, with W_{H2O}% decreasing from ~23% to ~11% as the film thickness increased from 1 to 6 μm (Figure 2d-iii, blue curve). This effect was likely missed in previous studies that used much larger thickness (*e.g.*, >100 μm).[12] Correspondingly, V_o increased from ~20 to ~100 mV (Figure 2d-iii, black curve), also showing a close correlation with the extracted ΔW_{H2O}% (Figure 2d-iv). A device made with a thin film assembled from poly(3,4-ethylenedioxythiophene) (PEDOT) nanowires[34] (Figure 2e-i; Figure S1, Supporting Information) also generated a spontaneous V_o~55 mV in the ambient environment (Figure 2e-ii). Consistent thickness-dependent trends in W_{H2O}% (Figure 2e-iii, blue curve), V_o (black curve), and V_o-ΔW_{H2O}% relationship were consistently observed (Figure 2e-iv).

The existence of the adsorption gradient was further confirmed by the direct observation of depth-dependent adsorption in the nanoporous materials. The resistance of the material layers showed monolithic increase with increasing buried depth (Figure 3a). Since film resistance was inversely related to moisture adsorption[9] (Figure 3b), these results demonstrate that water adsorption decreases with increasing depth, providing direct evidence of the existence of an adsorption gradient. Importantly, the decreasing adsorption in the buried layer was observed by gradually increasing the upper layer thickness. This reverse adsorption is not expected during a gradual hydration process and must be due to a dynamic equilibrium (Figure 1). This dynamic origin suggests that the gradient can sustain over time, which is inherently different from the temporary gradient observed during gradual hydration processes in other devices.[17-18, 21]

Note that both the top and bottom electrodes in all above devices were made from electrodes coated with inert Au. To avoid possible contamination from other metal element, pure Au electrodes were made by directly depositing a 50-nm Au layer (*i.e.*, without adhesion layer of other metal) on substrates. Devices fabricated from these pairs of pure Au electrodes yielded consistent electric outputs (Figure S3, Supporting Information). These results show that a wide diversity of materials can be used to make Air-gen devices to generate electricity in the ambient environment, which is not associated with electrochemical process in the electrode and is consistent with the generic picture proposed (Figure 1).

2.3. Comparison of material properties

Analyses of the Air-gen effect in these different nanoporous materials revealed several distinct trends (Figure 4). The saturation thickness (d_s), defined as the depth at which the adsorption reduces to 10% of the surface adsorption, trended with the pore size of materials (top, Figure 4). Larger pore sizes yielded larger d_s. This is consistent with the expectation that a larger lateral size needs to be compensated by a deeper depth to produce a confinement effect (Figure 1b). For this reason, we expect the adsorption gradient (∇_{H2O}), defined as ΔW_{H2O}% per unit thickness, to trend in the opposite direction as the pore size, consistent with observation (bottom, Figure 4, black curve).

Surface functionality can play key role in the water-solid interaction,[4] thereby substantially affecting the performance of the materials used. The nanoporous materials used generally contained hygroscopic surface functional groups and showed hydrophilic surface property (Figure S4, Supporting Information). The voltage 'density' or electric field (E), which is closely related to energy density, showed a deviation from the trend of ∇_{H2O} (bottom, Figure 4, blue curve). For example, protein nanowire films had a slightly lower ∇_{H2O} but a much higher E (*e.g.*, > 4 times) than the values observed for GOx films. This is because

E results from a charge gradient[19] that also depends on the surface functionality. A higher density of hygroscopic groups is expected to enhance the ionization/charge gradient at the same ∇_{H2O}. Protein nanowires have higher density of surface groups,[19] thus resulting in larger E. Overall, biomaterials tended to have a larger E/∇_{H2O} ratio (green dots) and, hence, energy efficiency than nonbiological materials (orange dots) (bottom Figure 4, inset). This finding is consistent with the expectation that biomaterials usually have more hygroscopic groups. Improving the hydrophilicity of the same CNF material by surface functionalization led to improved adsorption gradient and electric outputs (Figure S5, Supporting Information), which is consistent with the analysis above. Protein nanowire films had the largest E and, therefore, energy density (Figure S6, Supporting Information), which can be attributed to the small pore sizes in the films and the high density of surface hygroscopic groups on individual nanowire surfaces. The estimated conversion efficiency in different materials showed a trend consistent with that observed in the E/∇_{H2O} ratio (Table S1, Supporting Information).

To further test the generality of the Air-gen effect and investigate mechanistic trends, we used a thin film made from nanoporous anodic aluminum oxide (AAO) with relatively large pore size (~ 200 nm) to make a device (Figure S7, Supporting Information). The pore size is close to the boundary of observability for the Air-gen effect, as it is comparable to the mean free path of air-water molecules[26] and close to the upper limit for observable vapor pressure lowering.[24] As expected from the generic effect, the device generated a spontaneous $V_o \sim 45$ mV (Figure S7, Supporting Information). The E (~7.5 V/cm) of the device was the lowest among all the test materials. This result was anticipated based on the combined properties of the large pore size and low density of surface groups. Conversely, a porous film made from bristled microparticles[35] with a pore size above the micrometer scale produced negligible Air-gen effect (Figure S8, Supporting Information).

2.4. Current generation mechanism

Since porous materials assume a certain level of conductivity in the ambient environment,[36] the sustained voltage output indicates that there exists a continuous charging mechanism to balance the leakage. It is generally acknowledged that the details of surface charging are largely unknown.[37] The previous assumption of water-assisted deprotonation in surface functional groups has provided a reasonable description in some materials,[12, 19] although questions remain regarding how the current loop is closed (*e.g.*, internal proton current converts to external electron current). Another attempt introduced the concept of image electrons in the material to circumvent this challenge.[38]

Even though it is widely acknowledged that air water is the enabling factor for many humidity harvesters, a central question that has never been addressed is whether water is consumed during the process. We designed experiments to address this question critically related to Air-gen mechanism. In one set of experiment, the weight of an Air-gen device was real-time monitored during the current production. The Air-gen device maintained the same weight during the 110-h continuous current production (Figure S9, Supporting Information). In the other set of experiment, an Air-gen device was placed in a sealed chamber for current generation with the relative humidity (RH) constantly monitored (Figure S10a, Supporting Information). During a 58-h continuous current production, the total transferred charge, if to be provided by water consumption or net adsorption, would induce a RH change >4% in the chamber. However, the measured RH maintained a stable level (Figure S10b, Supporting Information). These results suggest that the current production in Air-gen does not involve net water adsorption or decomposition (*e.g.*, redox). This finding supports that 1) a dynamic water exchange (without net adsorption) and 2) an associated electrostatic/ionic charge transfer are responsible for the current production. This conclusion is consistent with the generic effect observed in various materials with which water is unlikely to react.

Therefore, the surface charging process can be viewed as a form of 'contact electrification' between water molecules and a solid interface. This view is consistent with the observation that surface charging by air humidity has been observed across a broad range of materials, including dielectrics and metals,[37] with a negative charge donation dominantly observed. Different charge species (*e.g.*, ions, electron, hole) may be involved in the electrification process with different material surfaces,[37] and the details warrant further study.

Based on the above considerations, we propose a mechanistic model for further understanding the Air-gen effect. The model is based on several key rationales. First, we assume that a water molecule/cluster assumes a certain level of charge negativity compared to a solid surface (Figure 5a). The detail of the responsible charge type is left out for reasons discussed above, which nonetheless does not affect the analysis and prediction. We show that the dynamic water exchange process (Figure 5a) can induce net (negative) charging to the solid interface (Figure S11, Supporting Information), in which a higher humidity can push the exchange equilibrium toward higher surface charging. This is consistent with the previous experimental observations that higher humidity levels led to larger surface potential.[37] This leads to the expectation that the outer layer of material, exposed to higher water exchange rates, will experience more surface charging than the inner layer (Figure 5b). This charging difference can be also understood from the view of gas-solid 'contact electrification', during which the outer material layer is subject to more contacts from water molecules than the inner layer (Figure 1). This is also consistent with the observation that the top electrodes of devices always assumed a negative voltage sign (Figure 2a-e (ii)). Second, the surface charging can further induce image charge in the material (Figure 5a). Importantly, the donated surface charge can be less mobile based on studies showing that a high humidity did not facilitate its dissipation,[37] leaving the image charge in material to be the main type for diffusion. We show a diffusion model based on the image charge to account for the voltage output V_o and its proportionality to the adsorption difference $\Delta W_{H2O}\%$ between the top and bottom film interfaces (Figure S12, Supporting Information). This is consistent with experimental observations that: 1) increasing film thickness (at fixed RH) led to expected increasing $\Delta W_{H2O}\%$ and thus increasing V_o in all the devices made from different nanoporous materials (Figure 2a-e (iv)); 2) RH change led to expected change in $\Delta W_{H2O}\%$ (at fixed film thickness) and thus change in V_o, with $\Delta W_{H2O}\%$ and V_o following the same trend in different devices (Figure S13a, b, Supporting Information). Note that the previous deprotonation model[19] can be included in this model by considering that the deprotonation is equivalent to negative charge donation, with proton being considered as the diffusive image charge. Third, the dynamic adsorption-desorption water exchange, with differentiated rate between the outer and inner interfaces, sustains the continuous charging difference to balance the leakage in material (*e.g.*, induced by V_o). This is supported by experiments that increasing the RH, hence the water exchange rate or charging rate, increased the current output (Figure S13c, Supporting Information), and blocking and resuming the water exchange reversibly switched the electric output (Figure S14, Supporting Information).

A 'leaky capacitor' model, based on above rationales, is proposed to substantiate the mechanistic description (Figure 5c, purple region). In this model, the continuous charging (more precisely the charging difference between the top and bottom interfaces) from air humidity is represented by a current source I_s; the resultant charge difference between the top and bottom electrodes is equated to charge stored in a capacitor (C); the route of leaky current (I_{leak}) induced by voltage output (V) is represented by a resistor (R^{dev}). Importantly, R^{dev} is the intrinsic carrier resistance in material but not the typically measured resistance containing multiple contributions (see details in Figure S15, Supporting Information).

This model can be used to describe the current generation behaviors in Air-gen devices. At any steady state, the charging current shall cancel the leaky current. In an open circuit, this yields a steady voltage output $V_o = I_s \cdot R^{dev}$ (*e.g.*, from $I_s = I_{leak} = \frac{V_o}{R^{dev}}$). An external load R_L introduces an additional 'leaky'

current corresponding to the measured current (I). The new steady state will produce a voltage output $V = \frac{R_L}{R^{dev}+R_L} \cdot V_o$ (*e.g.*, from $I_s = I_{leak} + I = \frac{V}{R^{dev}} + \frac{V}{R_L}$). This voltage reduction, corresponding to a reduction in charge storage in the capacitor C, will produce a discharging current featuring the typical decaying trend (Figure 5d, yellow region). Once the new steady state is reached, the measured current I will obey Ohm's law to yield a sustaining value $I = \frac{V}{R_L} = \frac{V_o}{R^{dev}+R_L} = \frac{R^{dev}}{R^{dev}+R_L} \cdot I_S$ (Figure 5d, green region), which is the result of the continuous charging I_s from the air humidity. Not surprisingly, disconnecting the external load will shut off the external leaky route and shift the dynamics to a net charging to C, which will restore the initial voltage.

Above predicted current behaviors were consistently observed in Air-gen devices made from different materials (Figure S16, Supporting Information). Representative result from an Air-gen made from GOx film showed that the current decayed within the first hour (Figure 5e, yellow region) but maintained a stable value for the following 12 h (green region). Disconnecting the two electrodes gradually restored the voltage output (black curve). The cycle was repeated beyond the test time of 10 days (Figure 5f). The current is unlikely to come from any internal redox process (Figure S17, Supporting Information), consistent with the experimental result that water was not consumed during the process (Figure S10, Supporting Information). This provides evidence that the main diffusion carrier type may be electron or hole (see details in Figure S15, Supporting Information), which does not require a redox in the material or at the electrode to sustain the closed-loop current flow. Together, the model and experimental results support a sustainable mechanism in Air-gen devices.

This sustainable mechanism is inherently different from the non-sustainable mechanism involved in previous devices,[17-18] in which gradual net adsorption (*i.e.*, hydration) in the materials induced a temporary gradient to induce current (*e.g.*, through the induction of an ionization gradient), but the current ceased once an adsorption saturation was reached. These devices could only offer a one-time current output no longer than 48 h.[17-18] All the devices tested here showed continuous current production in test window of one week (Figure S18, Supporting Information). In fact, the Air-gen device made from protein nanowires, which was kept in the ambient environment for over 3 years, still produced a similar voltage output (Figure S19, Supporting Information). These time spans are much longer than the typical hydration time, supporting the sustainable mechanism based on a dynamic equilibrium (Figure 5a, b). The Air-gen device is not a 'perpetual motion engine', because the energy comes from the electrostatic energy (not kinetic one) of discrete water molecules in a vast open source. The asymmetric device structure leads to differentiated contact rates (Figure 1) and thus, differentiated charging to the top and bottom interfaces from water molecules (Figure 5b) under dynamic equilibrium. The exchanging water molecules from the open air may be considered as an 'incidental' source, like light to a solar cell. If this exchange process was blocked by sealing the top interface, the energy output was stopped, but it resumed once the seal was removed (Figure S14, Supporting Information).

2.5. Heterogeneous Air-gen devices

The proposed mechanism readily predicts that connecting two materials with dissimilar charging capacity from air humidity will also yield a leaky capacitor that generates electricity. To demonstrate this, we connected GOx films to other films made from biomaterials (Figure 6a; Figure S20, Supporting Information) because they had distinct charging efficiency inferred from the E/∇_{H_2O} ratio (bottom, Figure 4, inset). All devices produced sustained V_o in the ambient environment (Figure 6b), with values considerably larger than those from devices of heterogeneous surface functionalization.[11-12] Material processing is easier, and the material choice is much broader. The GOx terminal always recorded a positive voltage with respect to the biomaterial terminal, consistent with the expectation that biomaterials have better charging efficiency (bottom, Figure 4, inset).

To further substantiate the mechanistic picture, we conducted another test where GOx films of different thicknesses were vertically stacked on a film (0.9 μm thick) made from protein nanowires[14, 19, 39] (Figure 6c; Figure S21, Supporting Information). At a reduced thickness (~1.2 μm), the GOx film is not expected to substantially block water exchange in the bottom layer. The protein nanowire layer thus could still be charged more than the GOx layer, resulting in a substantial V_o ~ 150 mV (Figure 6d-i). Increasing the GOx film thickness (~2.4 μm) is expected to reduce the charging in the nanowire layer, leading to a decreased V_o ~30 mV (Figure 6d-ii). Further increasing the GOx film thickness (~3.6 μm) reduced the charging in the nanowire layer to be below that in the GOx film, resulting in a reverse V_o ~ -130 mV (Figure 6d-iii). The varying amplitude also indicates that the voltage output is not a chemical battery effect between different materials. These results provide not only strong support for the proposed mechanistic model but also offer broad engineering strategies for the Air-gen technology.

3. Conclusion

In summary, we have revealed a generic Air-gen effect across a broad range of inorganic, organic and biological materials. The generic effect is attributed to differentiated dynamic water exchange and associated charge exchange in nanoporous materials, which manifests as the existence of a self-maintained water adsorption gradient. A pore size below the mean free path of air water (~100 nm) is expected to yield a prominent effect. Surface functional groups are important in determining the exchange dynamics, with hygroscopic groups generally expected to facilitate the effect. Together, smaller pores and a higher density of hygroscopic groups are expected to yield higher energy density, as demonstrated among the materials studied. However, excessive water adsorption may lead to surface wetting, which can flatten out the gradient essential to the effect. Therefore, superhydrophilic materials may not necessarily be the best candidate. Biomaterials are usually made from amphiphilic biomolecules, indicating that an amphiphilic surface may be preferred for an enhanced effect. Metal organic frameworks (MOFs) can be another promising class of materials for Air-gen applications, due to their well-defined nanoporosity and ability to incorporate hygroscopic functional groups for water adsorption.[40] Scalable, high-quality MOF thin films featuring low-density grain boundaries (*e.g.*, to effectively reduce uncontrolled extrinsic pores at the boundaries) are needed to fully harness their intrinsic structural properties, which may require further synthetic improvement.[41] Although the molecular detail of surface charging is not fully known and differ between different materials, the proposed 'leaky capacitor' model offers good understanding of the energy generation behaviors, as well as providing useful guidance for developing and optimizing devices. We expect that the work will greatly expand the potential of the Air-gen technology.

The sustainable Air-gen technology holds promising prospect. Although a single sheet of Air-gen has a lower energy output (*e.g.*, up to μW/cm^2 level) than some existing harvesters (Table S2, Supporting Information), they may be vertically stacked to improve power without taking up additional footprint due to the diffusive nature of humidity. A preliminary study showed that an Air-gen device placed in an airgap of commeasurable size to device thickness (*e.g.*, 20 μm) could retain electric output.[19] This leads to an estimated energy density > 1 kW/m^3 in vertically integrated Air-gen (although this value is still subject to the available energy flow in the environment). Importantly, since air humidity is ubiquitous and continuous 24/7, Air-gen can be deployed almost anywhere for continuous energy harvesting, transcending the inherent intermittence of existing harvesters restricted to time or location (Table S2, Supporting Information). Air-gen offers flexibility in material choice (*e.g.*, renewable production) and engineered form factor (*e.g.*, to merge with the environment), making it a possible 'greener' energy technology for the future.

4. Experimental Section

Material preparation: PEDOT nanofibers were synthesized by using a soft-template approach reported previously.[34] Briefly, the templates were formed by adding 30 mM $FeCl_3$ solution into 30 mM sodium dodecyl sulfate (SDS, Sigma-Aldrich) solution at 50°C. 10 mM 3,4-Ethylenedioxythiophene (EDOT, Tokyo Chemical Industry Co., Ltd.) monomers were then slowly introduced into the solution with continuous stirring for 6 h. The obtained nanofibers were washed by repeated process of centrifugation (5000 rpm, 20 min) and redispersion in methanol and water**.** Silk fibroin (SF) was extracted from silkworm cocoons (Oregon Silkworms) following a procedure described previously.[32] Briefly, silk cocoons (5 g) were boiled in 0.02 M Na_2CO_3 for 30 min. The obtained fibers were rinsed in deionized (DI) water (20 min, 3 times) and dried overnight. The raw silk fibroin was then dissolved in 9.3 M LiBr (Acros Organics™) and incubated at 60 °C for 4 h. The solution was dialyzed in DI water for 48 h. Wild-type *G. sulfurreducens* was grown as previously described under anaerobic conditions with acetate as the electron donor and fumarate as the electron acceptor.[42] Protein nanowires were synthesized and harvested following previous method.[19] Cellulose nanofibrils (3 wt % in water, Cellulose Lab) and graphene oxide (0.4 wt % in water, MSE Supplies™) were commercially produced.

Device fabrication: The bottom electrode (Ti/Au, 5/30 nm, 1×15 mm^2) was patterned by a shadow mask and defined with standard metal deposition on a glass slide (25 × 75 mm^2; Fisher Scientific). A 5 × 5 mm^2 area was defined by scotch tape. Solution containing the material of interest was drop-casted in the defined area and dried at ~80 ºC to form the thin film. The film thickness was controlled by solution volume. For *G. sulfurreducens* biofilm, a polyimide substrate patterned with Au electrode was placed on a filter paper (42.5 mm dia., 8 µm pore size; Whatman). The *G. sulfurreducens* culture solution was filtered through the paper to form biofilm on electrode. A braided gold-plated shield (~ 0.7 mm diameter, model CC-SC-50; LakeShore) was used as the top electrode for all the films for electrical measurements.

For (planer) heterojunction device, a pair of carbon electrodes (1× 15 mm^2) were defined by a laser writer (LaserPro Spirit GLS; GCC) on a polyimide substrate. Scotch tape was used to define the area (2 × 5 mm^2) for each material before film deposition. For the vertical device, the carbon electrodes were defined the same way on a polyimide substrate. Thin films were deposited on one of the electrodes by dropcasting. The other carbon electrode was cut into thin stripe (1×15 mm^2) and placed on top of the film layers to serve as the top electrode.

Humidity control: The tuned RH in some experiments was controlled by tuning the concentration of calcium chloride solutions[43] and monitored by a hygrometer (model 8706; Reed Instruments).

Measurement of moisture adsorption: The moisture adsorption in thin films was measured by a quartz crystal microbalance (CHI 440, CH Instruments). The film was deposited on the quartz crystal resonator by dropcasting. The film weight was initially measured at a controlled humidity of 50% and then at humidity ~0% (by flowing dry air). The weight difference corresponded to the weight of adsorbed water.

Characterizations: The SEM images were acquired by using a JSM-7001F system. Film thicknesses were determined by a 3D profiler (NewView™ 9000; Zygo). The voltage and current outputs were measured by using a source meter (Keithley 2401; Tektronix) interfaced with computerized recording software. The measurements were performed in the ambient environment, unless otherwise specified.

FIGURES

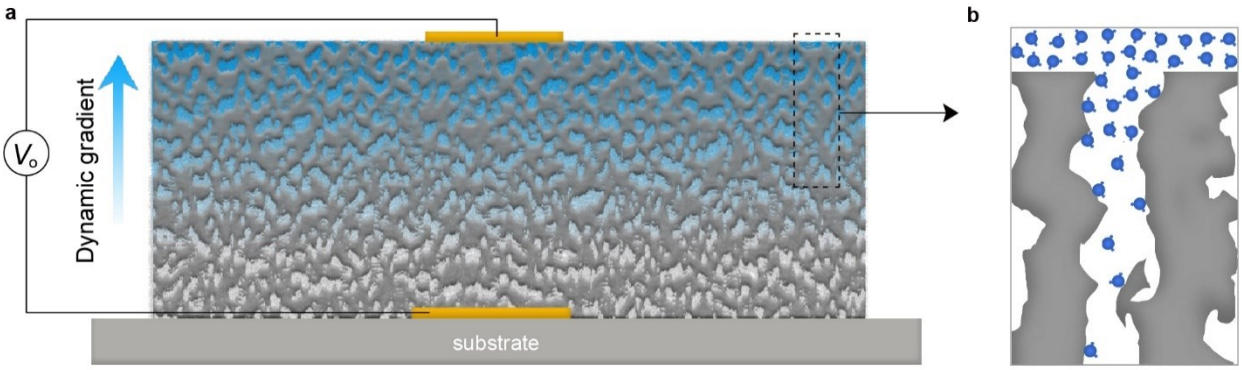

Figure 1. Air-gen device structure. a) Schematic of the Air-gen device made from a nanoporous thin film sandwiched between a pair of inert (*e.g.*, Au) electrodes. The top electrode has relatively small size to permit air exposure. A stable water adsorption gradient (blue trend) resulted from dynamic equilibrium is induced across the film thickness. b) Zoom-in schematic of the confined nanoscale channel inducing a concentration gradient in air-water molecules (blue).

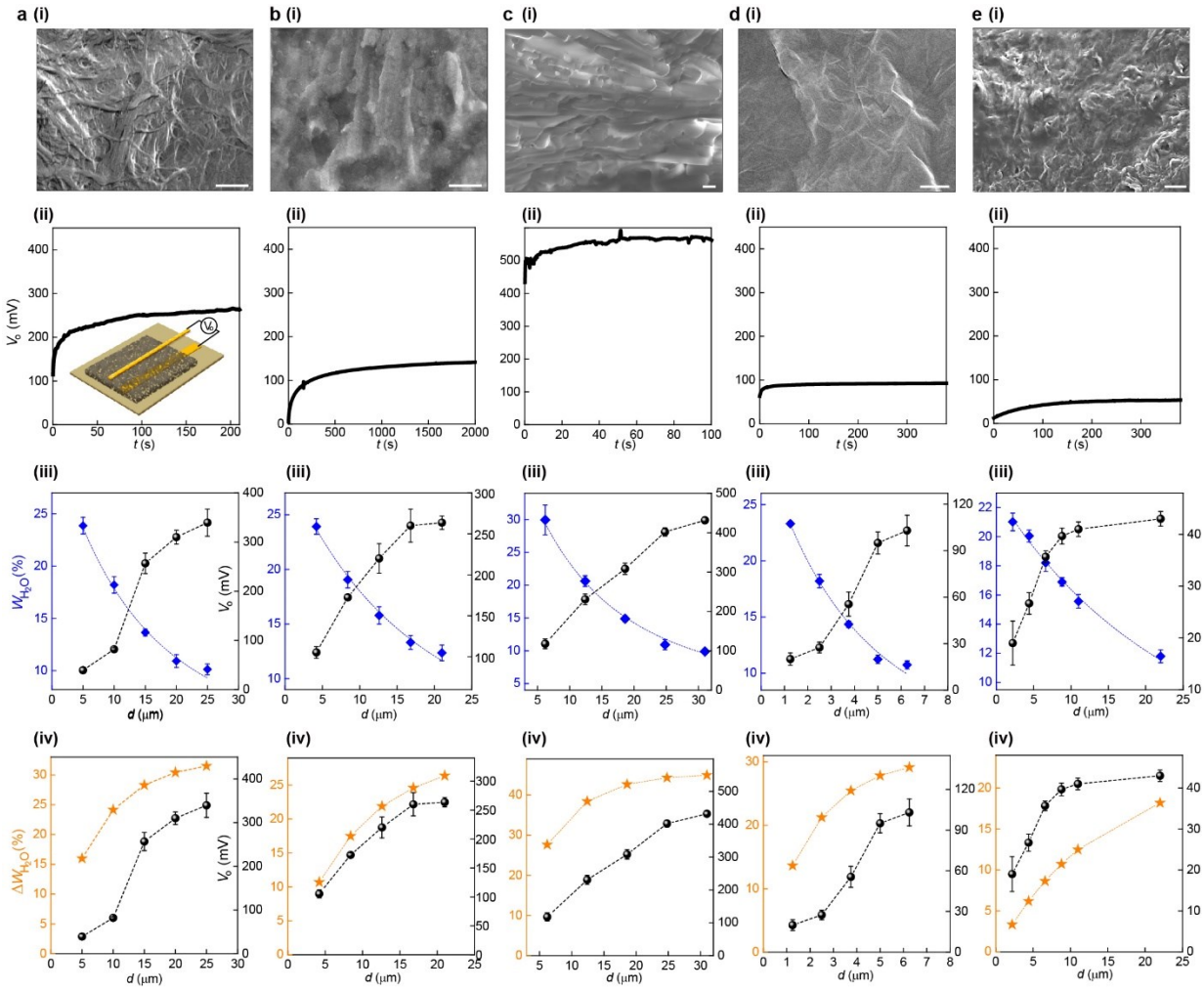

Figure 2. Air-gen effect in different materials. a-e) (i) Scanning electron microscope (SEM) images of thin-film surfaces made from CNF, SF, *G. sulfurreducens*, GOx, and PEDOT nanowires, respectively. Scale bars, 1 μm. (ii) Representative open-circuit voltage (V_o) in devices made from CNF film (25 μm thick), SF film (21 μm thick), *G. sulfurreducens* biofilm (31 μm thick), GOx film (6 μm thick), and PEDOT film (11 μm thick), respectively. All the devices shared the same structure (inset) and same size (0.5 × 0.5 cm^2). (iii) Thickness (d)-dependent water adsorption W_{H2O}% (blue curve) and V_o (black curve) in CNF films, SF films, *G. sulfurreducens* biofilms, GOx films, and PEDOT films, respectively. For fitting (blue dashed line), the local adsorption at depth d is approximated by $f(d) = A \cdot e^{-\frac{d}{\lambda}}$, where A and λ are the top-interface adsorption and characteristic thickness, respectively. Then the fitting value of average adsorption (corresponding to measured W_{H2O}%) is $\overline{f(d)} = \frac{\lambda \cdot A}{d} \cdot (1 - e^{-\frac{d}{\lambda}})$. (iv) Fitting adsorption difference $\Delta W_{H2O}\% = A \cdot (1 - e^{-\frac{d}{\lambda}})$ between the top and bottom interfaces (orange) and measured V_o (black) with respect to film thicknesses d in devices made from CNF films, SF films, *G. sulfurreducens* biofilms, GOx films, and PEDOT films, respectively. All the measurements were performed in the ambient environment with a RH ~50%. All the error bars are standard deviations ($n \geq 3$).

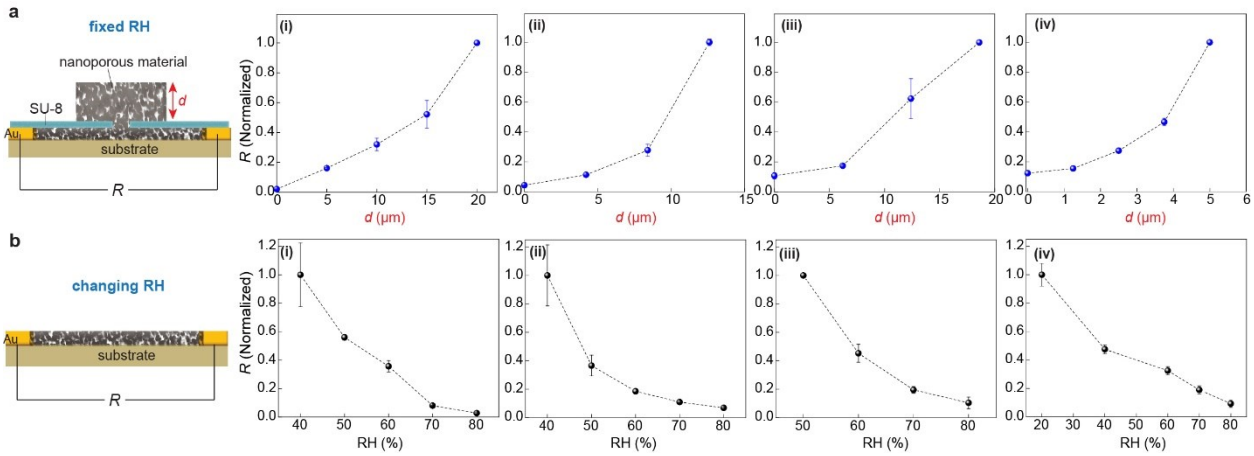

Figure 3. Depth-dependent (dynamic) water adsorption in nanoporous films**.** a) (Left) Schematic of the experimental setup, in which a thin layer (~ 1 μm thick, 1×1 cm^2) of nanoporous film is deposited on a Si/SiO_2 substrate and electrically addressed by a pair of Au electrodes (for resistance measurement). A water-impermeable thin layer (SU-8, ~ 2 μm thick) is covered on the thin film, with a small opening (1×1 mm^2) connecting to the top layer of the same nanoporous material. This small opening allows moisture diffusion but minimizes the conduction contribution from the top layer to the bottom layer. Therefore, the change of resistance (*R*) in the bottom thin layer, if any, would be mainly induced by the change of water adsorption in that layer. (Right) Monolithic increase in *R* with the increase of buried depth (*d*, or top-film thickness) in thin films made from (i) CNF, (ii) SF, (iii) *G. sulfurreducens*, and (iv) GOx, respectively. The RH (~80%) was kept constant during the measurements. b) Monolithic decrease in *R* in thin films directly exposed to air (left schematic) with the increase of RH, consistent with general observation in thin-film materials.[9] All the error bars are standard deviations ($n \geq 3$).

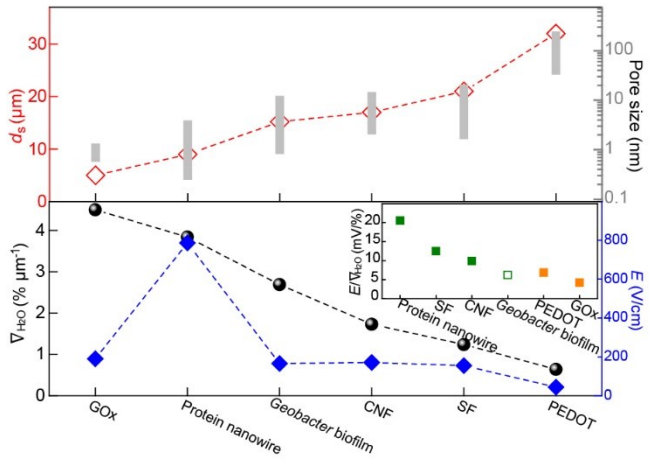

Figure 4. Comparison of parameters in Air-gen devices made from different nanoporous materials. (Top) Saturation thickness d_s (orange) with respect to pore-size range (gray) in different materials. d_s, defined as the depth at which the water adsorption reduces to 10% of the top-interface adsorption, corresponds to 2.3λ extrapolated from Figure 2 a-e (iii). The pore-size ranges in different materials were obtained either by imaging or from previous reports.[19],[31-34] (Bottom) Adsorption gradient ∇_{H2O} (black) and generated electric field E (blue) in different materials. The values were calculated based on data in Figure 2. (Inset) Calculated E/∇_{H2O} ratio in different materials, with the green and orange dots indicating biomaterials and nonbiological materials, respectively. The *G. sulfurreducens* biofilm (open green) has reduced E/∇_{H2O} compared to other biomaterials, likely due to that the relatively large grain of cell body reduces the efficiency. The data in protein nanowire films was obtained from previous study.[19]

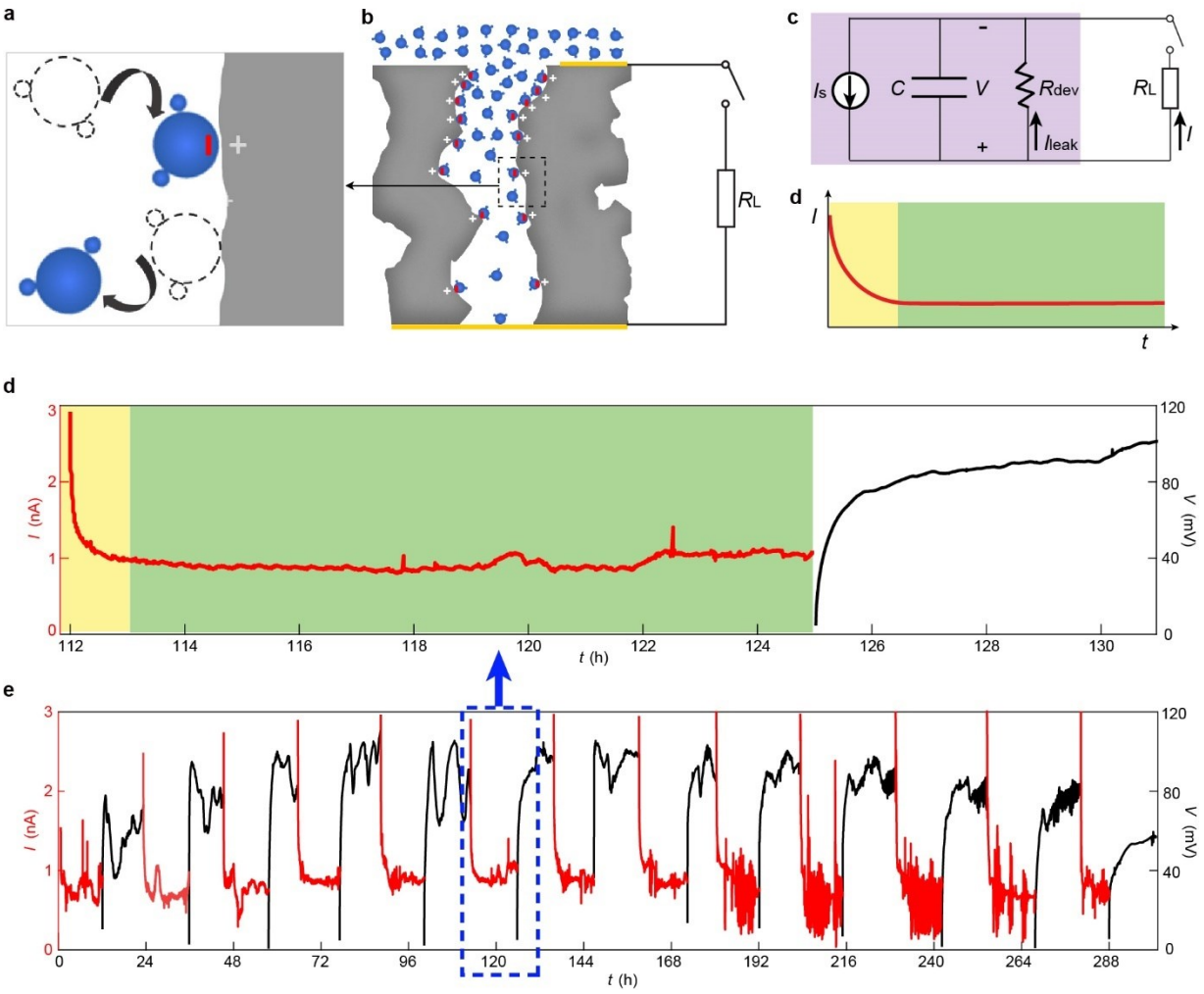

Figure 5. Current generation in Air-gen device. a) Schematic of charge donation and induction associated with the dynamic water (blue) exchange at the solid interface (gray). b) Schematic of charging in the nanoporous material. The top layer is donated with more charge than the bottom layer due to the dynamic density gradient of water molecules. c) A proposed leaky capacitor model (purple region) for the Air-gen device. d) Qualitative current behavior from the circuit model in (c) when the switch is closed (t = 0). e) Measured current I (red curve) from an Air-gen device made from GOx (0.5×0.5 cm^2, 6 μm thick) when the top and bottom electrodes were short-circuited. The measured voltage V (black) gradually restored to the original open-circuit value when the two electrodes were disconnected. e) Continuous discharging-and-charging cycles measured in the same Air-gen device in (d). The measurements were carried out in the ambient environment with RH ~50%.

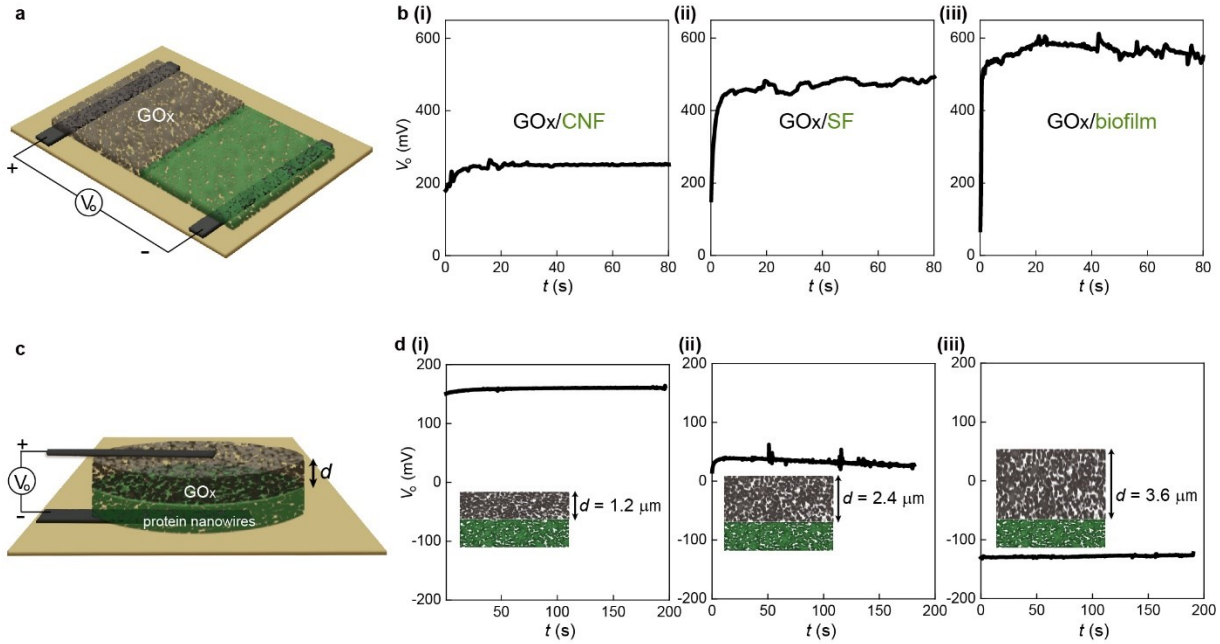

Figure 6. Heterogeneous Air-gen devices. a) Schematic of a heterogeneous Air-gen device made from a GOx thin film (2×5 mm^2, 1.2 μm thick) connected to another thin film (green) made from biomaterials (2×5 mm^2), with each film sitting on an inert carbon electrode. b) Open-circuit voltage V_o measured from heterogeneous Air-gen devices with the biomaterial films made from (i) CNF (5 μm thick), (ii) SF (4.2 μm thick), and (iii) *G. sulfurreducens* biofilm (6.2 μm thick), respectively. c) Schematic of a vertical heterogeneous Air-gen device made from a GOx film stacked on a protein nanowire film. d) V_o measured from vertical heterogeneous Air-gen devices with varied GOx thicknesses of (i) 1.2 μm, (ii) 2.4 μm, and (iii) 3.6 μm, respectively. All the measurements were performed in the ambient environment with RH ~ 30%.

Supporting Information

Supporting information is available from the Wiley Online Library or from the author.

Acknowledgements

J.Y. acknowledges support from the National Science Foundation (NSF) DMR2027102 and Sony Group through the Sony faculty innovation award. X.L. acknowledges support from the Link Foundation Energy Fellowship. J.Y. also acknowledges supports from NSF CAREER CBET-1844904. The authors thank Prof. Derek Lovley for helpful comments on the manuscript and Dr. Toshiyuki Ueki for supply of nanowire materials. Part of the device fabrication work was conducted in the clean room of the Center for Hierarchical Manufacturing (CHM), an NSF Nanoscale Science and Engineering Center (NSEC) located at the University of Massachusetts Amherst.

Conflict of Interest

The authors declare no conflict of interest.

Author contributions: J.Y. and X.L. conceived the project and designed experiments. X.L. carried out experimental studies in material characterization, device fabrication and electrical measurement. H.Y. and L.S. helped with material characterization. J.Y. performed analyses, proposed models, oversaw the project, and wrote the manuscript.

Data Availability Statement

Data that support the findings of this study are available in the supporting information; additional data is available from the corresponding author upon reasonable request.

Keywords

electricity, humidity, hydrovoltaic, energy harvesting, sustainable

References

[1] D. Gielen, F. Boshell, D. Saygin, M. D. Bazilian, N. Wagner, R. Gorini, *Energy Strateg Rev* **2019**, 24, 38.
[2] J. A. Paradiso, T. Starner, *Ieee Pervas Comput* **2005**, 4, 18.
[3] C. S. Kaunda, C. Z. Kimambo, T. K. Nielsen, *ISRN Renewable Energy* 2012, **2012**, 730631.
[4] D. Shen, W. W. Duley, P. Peng, M. Xiao, J. Y. Feng, L. Liu, G. S. Zou, Y. N. Zhou, *Adv Mater* **2020**.
[5] Z. H. Zhang, X. M. Li, J. Yin, Y. Xu, W. W. Fei, M. M. Xue, Q. Wang, J. X. Zhou, W. L. Guo, *Nat Nanotechnol* **2018**, 13, 1109.
[6] Y. X. Zhang, D. K. Nandakumar, S. C. Tan, *Joule* **2020**, 4, 2532.
[7] Z. Sun, X. Wen, L. Wang, D. Ji, X. Qin, J. Yu, S. Ramakrishna, *eScience* **2022**, 2, 32.
[8] F. Zhao, H. H. Cheng, Z. P. Zhang, L. Jiang, L. T. Qu, *Adv Mater* **2015**, 27, 4351.
[9] X. M. Liu, T. D. Fu, J. Ward, H. Y. Gao, B. Yin, T. Woodard, D. R. Lovley, J. Yao, *Adv Electron Mater* **2020**, 6.

[10] X. M. Liu, T. Ueki, H. Y. Gao, T. L. Woodard, K. P. Nevin, T. D. Fu, S. Fu, L. Sun, D. R. Lovley, J. Yao, *Nat Commun* **2022**, 13, 4369.
[11] K. Liu, P. H. Yang, S. Li, J. Li, T. P. Ding, G. B. Xue, Q. Chen, G. Feng, J. Zhou, *Angew Chem Int Edit* **2016**, 55, 8003.
[12] H. H. Cheng, Y. X. Huang, F. Zhao, C. Yang, P. P. Zhang, L. Jiang, G. Q. Shi, L. T. Qu, *Energ Environ Sci* **2018**, 11, 2839.
[13] Y. X. Zhang, S. Guo, Z. G. Yu, H. Qu, W. X. Sun, J. C. Yang, L. Suresh, X. P. Zhang, J. J. Koh, S. C. Tan, *Adv Mater* **2022**, 34, 2201228.
[14] Y. Zhang, Z. Yu, H. Qu, S. Guo, J. Yang, S. Zhang, L. Yang, S. Cheng, J. Wang, S. C. Tan, *Adv Mater* **2023**, 2208081, DOI: 10.1002/adma.202208081
[15] S. Zhou, A. Bongiorno, *Sci Rep* **2013**, 3, 2484.
[16] R. Foudazi, R. Zowada, I. Manas-Zloczower, D. L. Feke, *Langmuir* **2023**, 39, 2092.
[17] J. X. Bai, Y. X. Huang, H. Y. Wang, T. L. Guang, Q. H. Liao, H. H. Cheng, S. H. Deng, Q. K. Li, Z. G. Shuai, L. T. Qu, *Adv Mater* **2022**, 34, 2103897.
[18] H. Y. Wang, Y. L. Sun, T. C. He, Y. X. Huang, H. H. Cheng, C. Li, D. Xie, P. F. Yang, Y. F. Zhang, L. T. Qu, *Nat Nanotechnol* **2021**, 16, 811.
[19] X. M. Liu, H. Y. Gao, J. E. Ward, X. R. Liu, B. Yin, T. D. Fu, J. H. Chen, D. R. Lovley, J. Yao, *Nature* **2020**, 578, 550.
[20] T. D. Fu, X. M. Liu, S. Fu, T. Woodard, H. Y. Gao, D. R. Lovley, J. Yao, *Nat Commun* **2021**, 12, 3351.
[21] A. T. Liu, Y. Kunai, A. L. Cottrill, A. Kaplan, G. Zhang, H. Kim, R. S. Mollah, Y. L. Eatmon, M. S. Strano, *Nat Commun* **2021**, 12, 3415.
[22] T. Ueki, D. J. F. Walker, T. L. Woodard, K. P. Nevin, S. S. Nonnenmann, D. R. Lovley, *ACS Synth Biol* **2020**, 9, 647.
[23] Y. Lekbach, T. Ueki, X. M. Liu, T. Woodard, J. Yao, D. R. Lovley, *Biosens Bioelectron* **2023**, 226, 115147.
[24] C. K. Ho, in *Theory and Applications of Transport in Porous Media*, Vol. 20 (Eds: C.K. Ho, S.W. Webb), Springer, Dordrecht **2006**.
[25] I. Langmuir, *J Am Chem Soc* **1932**, 54, 2798.
[26] M. J. Tang, M. Shiraiwa, U. Poschl, R. A. Cox, M. Kalberer, *Atmos Chem Phys* **2015**, 15, 5585.
[27] H. Pang, W. S. Dai, M. Xie, *J Phys a-Math Theor* **2011**, 44, 365001.
[28] A. Sisman, Z. F. Ozturk, C. Firat, *Phys Lett A* **2007**, 362, 16.
[29] A. Sisman, I. Muller, *Phys Lett A* **2004**, 320, 360.
[30] G. P. Ren, Z. Wang, B. T. Zhang, X. Liu, J. Ye, Q. C. Hu, S. G. Zhou, *Nano Energy* **2021**, 89, 106361.
[31] Q. G. Zhang, C. Deng, F. Soyekwo, Q. L. Liu, A. M. Zhu, *Adv Funct Mater* **2016**, 26, 792.
[32] A. Marquez, M. V. Santos, G. Guirado, A. Moreno, S. D. Aznar-Cervantes, J. L. Cenis, S. H. Santagneli, C. Dominguez, F. G. Omenetto, X. Munoz-Berbel, *Lab on a Chip* **2021**, 21, 608.
[33] T. Liu, L. Tian, N. Graham, B. Yang, W. Z. Yu, K. N. Sun, *Environ Sci Technol* **2019**, 53, 11949.
[34] M. G. Han, S. H. Foulger, *Small* **2006**, 2, 1164.
[35] B. Yin, X. M. Liu, H. Y. Gao, T. D. Fu, J. Yao, *Nat Commun* **2018**, 9, 5161.
[36] A. Revil, P. W. J. Glover, *Phys Rev B* **1997**, 55, 1757.
[37] C. A. Rezende, R. F. Gouveia, M. A. da Silva, F. Galembeck, *J Phys-Condens Mat* **2009**, 21, 263002.
[38] Y. S. Qin, Y. S. Wang, X. Y. Sun, Y. J. Li, H. Xu, Y. S. Tan, Y. Li, T. Song, B. Q. Sun, *Angew Chem Int Edit* **2020**, 59, 10619.
[39] D. R. Lovley, J. Yao, *Trends Biotechnol* **2021**, 39, 940.
[40] W. T. Xu, O. M. Yaghi, *ACS Central Sci* **2020**, 6, 1348.
[41] Z. H. Fu, G. Xu, *Chem Rec* **2017**, 17, 518.
[42] M. V. Coppi, C. Leang, S. J. Sandler, D. R. Lovley, *Appl Environ Microb* **2001**, 67, 3180.
[43] R. H. Stokes, R. A. Robinson, *Ind Eng Chem* **1949**, 41, 2013.